Bollettino di Geofisica Teorica ed Applicata Vol. 59, n. 1, pp. 47-70; March 2018
DOI 10.4430/bgta0223

Analysing the influence of different elastic parameterizations in AVA-petrophysical inversion and in litho-fluid facies classification for a reservoir located in offshore Egypt

M. Aleardi

Earth Sciences Department, University of Pisa, Italy

(Received: September 18, 2017; accepted: January 18, 2018)

ABSTRACT I study the influence of different elastic parametrizations in amplitude versus angle (AVA)-petrophysical inversion and in litho-fluid facies identification with a focus on a reservoir located in offshore Egypt. Concerning the AVA-petrophysical inversion, I first use linear rock-physics models (RPMs) to rewrite the AVA forward modelling in terms of petrophysical properties instead of elastic properties. After demonstrating the reliability and the prediction capabilities of the derived RPMs, I apply a Bayesian inversion to estimate petrophysical properties from the analytical AVA responses derived from the logged elastic attributes pertaining to a blind well. Then, the standard sensitivity analysis tools are used to theoretically investigate the results provided by the AVA-petrophysical inversion and to examine the differences between the derived petrophysical-AVA forward operators. As regards the litho-fluid facies identification, I verify if different elastic parameterizations yield different classification results. For the considered reservoir, it results that the different elastic parameterizations do not influence the AVA-petrophysical inversion in which the porosity is always the best resolved parameter, whereas shaliness and water saturation are less resolvable. The results also show that different elastic parameterizations provide identical facies classification results.

Key words: AVA inversion, AVA-petrophysical inversion, litho-fluid facies classification, elastic parameterizations, sensitivity analysis.

1. Introduction

Numerical reservoir models are used by the exploration and production industry to plan new wells, calculate hydrocarbon reserves and predict production profiles. However, due to sparse well coverage, reservoir models are often poorly constrained at some distance from well locations. For this reason, a key challenge for reservoir geoscientists is the quantitative integration of 3D seismic data to obtain a more accurate representation of reservoir characteristics away from wells (Doyen, 2007). This process, usually called seismic-reservoir characterization, uses pre-stack seismic data to infer petrophysical rock properties and litho-fluid facies around the target area (Avseth *et al.*, 2005; Bosch *et al.*, 2010). However, it is known that seismic data do not provide direct information about reservoir properties or litho-fluid facies, but instead reflect

the elastic contrasts in the subsurface (i.e. contrasts in P-wave velocity, *Vp*; S-wave velocity, *Vs*; density, ρ). For this reason, seismic-reservoir characterization is usually a multi-step procedure. First, elastic parameters are estimated from seismic data by means of an inversion procedure. Then, the outcomes of this elastic inversion are converted into petrophysical properties (i.e. porosity, shaliness, water saturation) or used to infer litho-fluid classes (i.e. shale, brine-saturated sand, gas-saturated sand). Therefore, in seismic-petrophysical inversion a rock-physics model (RPM) is needed to link elastic parameters to petrophysical properties, whereas litho-fluid facies identification requires a transfer function or a classification algorithm that associates the elastic properties to a given litho-fluid class.

The elastic inversion step can be performed using complex inversion algorithms, such as full-waveform inversion (Bachrach *et al*., 2004; Aleardi and Mazzotti, 2017), or using methods that are less computationally intense, such as the amplitude versus angle (AVA) approach (Riedel and Theilen, 2001; Buland and Omre, 2003; Mazzotti and Zamboni, 2003). The AVA approach is particularly attractive not only for its limited computational effort, but also for its reliability that has been demonstrated worldwide over the last three decades (Ostrander, 1984; Rutherford and Williams, 1989; Mazzotti, 1990). Most common AVA inversion approaches are based on a linear approximation of the exact, non-linear, Zoeppritz (1919) equations that fully describe the reflection and transmission coefficients for a plane wave incident on a planar reflecting interface separating two homogeneous and isotropic half spaces. However, the Zoeppritz (1919) equations are so algebraically complex that it is difficult to intuitively grasp the physics of the AVA phenomenon. In addition, the non-linearity of these equations complicates their use for AVA analysis and AVA inversion. For these reasons, numerous approximations of the Zoeppritz (1919) equations have been published over the years. For example, popular versions are due to Bortfeld (1961), Richards and Frasier (1976), Aki and Richards (1980), Shuey (1985), Gidlow *et al*. (1992), Fatti *et al*. (1994), Verm and Hilterman (1994), and Gray *et al*. (1999). Each one of these approximations is based on a different elastic parameterization of the AVA forward modelling (i.e. in terms of seismic velocities and density; in terms of seismic impedances and density; in terms of Lamè moduli and density), but from the mathematical point of view, not all parameterizations of the Zoeppritz (1919) equations are equal. In particular, Debski and Tarantola (1995) analysed the probability density functions associated with AVA inversion for different choices of parameter sets. They found that choosing the parameter set (density, P-velocity, and S-velocity) to invert AVA information is not correct, although this happens to be a common choice. They proposed several better alternatives, for example: (density, P-impedance, Poisson's ratio), (density, P-impedance, S-impedance), or (density, P-impedance, Jussieu's ratio), where Jussieu's ratio is defined as the ratio of bulk modulus over shear modulus. In other words, according to Debski and Tarantola (1995), finding a good parameter choice corresponds to the search for maximally decoupled (independent) parameters. However, as far as the author is aware, the analysis of the effects of different elastic parameterizations in the AVA-petrophysical inversion has not been extensively discussed yet.

In addition, many authors [Goodway *et al*. (1997), Goodway (2001), Gray (2002) among many others] have stressed the importance to perform the litho-fluid facies identification using an alternative parameterization than the usual *Vp*, *Vs* and density ρ. Indeed, according to these authors, it is easier to understand the connection of reservoir parameters to fundamental rock properties, such as compressibility and rigidity, than it is to understand their connection to

traditional seismic attributes, like seismic velocities or impedances. In particular, according to Goodway *et al*. (1997), the combined use of the two Lamé parameters λ and μ would produce an improved identification of reservoir zones. The λ parameter is more affected by the fluid saturation, whereas the μ value is entirely independent from the saturating fluid and only affected by the properties of the rock matrix. Therefore, the combined use of these parameters, together with the density information, in a cross-plot of $\lambda\rho$ versus $\mu\rho$, allows for a better discrimination of different litho-fluid facies because it isolates lithologic properties (e.g. sand, shale, and carbonate facies) from fluid properties (brine, oil, gas). The theoretical reason that makes the $\lambda\rho$-$\mu\rho$ domain better discriminating than different domains (e.g., *Vp*-*Vs*), is that the Lamé parameters are independent (orthogonal) from one another, differently from the *Vp* and *Vs* values that are mutually correlated.

This work is aimed at investigating the influence of different elastic parameterizations in AVA-petrophysical inversion and in litho-fluid facies identification. In particular, I focus on a clastic, gas-saturated, reservoir located in offshore Egypt. The targets are gas-bearing sands at the depth range of 2300-2700 m that pertain to the slope-channel systems of Plio-Pleistocene age. Layering is typically at the centimetre scale, and the reservoir mainly consists of rather clean sand layers interbedded with laminated, non-permeable shales. As concerns the AVA-petrophysical inversion, I use the available well-log data to derive linear empirical rock-physics models for the investigated area that link each considered elastic parameter to the petrophysical properties of interest (porosity, water saturation, and shaliness). Several techniques are used to assess the suitability of the derived rock-physics relationships for reservoir characterization in the investigated area: first, I analyse the linear correlation coefficients between actual and predicted elastic properties; secondly, I use rock-physics templates to check if the predicted RPMs are able to reliably reproduce the actual influence played by each petrophysical property on the elastic parameters. Then, I use the derived linear RPMs to rewrite four popular linear approximations of full Zoeppritz (1919) equations in terms of petrophysical properties instead of elastic properties. This provides four linear petrophysical-AVA forward operators, each one derived from a specific elastic parameterization, that directly link the amplitude versus angle variations of the P-wave reflection coefficients (*Rpp*) to the contrasts in the petrophysical properties at the reflecting interface. These petrophysical-AVA forward operators are used to further prove the prediction capabilities of the derived RPMs and to rapidly check the effects of different elastic parameterizations on the outcomes of AVA-petrophysical inversion. In this inversion, the petrophysical properties are inferred from the analytical *Rpp* responses estimated from the logged *Vp*, *Vs*, and ρ values pertaining to a blind well that is a well not previously used to define the RPMs. The inversion is set in a rigorous Bayesian frame that provides a direct glimpse into the influence of the different elastic parameterizations in determining the petrophysical properties and their associated uncertainties. The inversion results, yielded by each petrophysical-AVA forward operator, are quantitatively assessed by computing the coverage probability ratio and the root-mean-square errors (RMSE) between actual and predicted properties. To theoretically investigate the results achieved by the AVA-petrophysical inversion, I analyse the four linear petrophysical-AVA forward modellings by using the well-known sensitivity analysis tools: unit covariance matrix, SVD decomposition, eigenvector analysis. This theoretical exercise allows getting a better understanding of the physical meaning of the derived petrophysical-AVA forward operators and to examine their differences in terms of expected resolution on model parameters and of error propagation from the data to the model space. In particular, the assumption of linear RPMs makes it possible to perform a sensitivity

analysis without the need to invert the data (i.e. the *Rpp* response). Indeed, the outcomes of the sensitivity analysis of the linear forward operators are entirely data-independent (Menke, 2012).

The second part is focused on the litho-fluid facies classification of well-log data. In this case, I use the logged *Vp, Vs*, and ρ values pertaining to the blind well to derive all the other considered elastic attributes that will constitute the input for a deterministic classification process based on quadratic discriminant analysis. For each considered combination of elastic characteristics, the classification results obtained on the blind well are qualitatively evaluated by comparing actual and predicted facies profiles. In addition, the contingency analysis tools [reconstruction rate, recognition rate and estimation index; Sammut and Webb (2011)] are used for a more quantitative assessment of the classification outcomes. For the investigated reservoir, the classification process is particularly challenging due to the significant overlap between the elastic characteristics of the different facies. This peculiarity can be explained taking into account the significant depth interval where the reservoir zone is located (2300-2700 m). Indeed, it is well known (Avseth *et al.*, 2003) that the elastic properties of sand and shale are increasingly similar with greater burial depth. In addition, large depths stiffen the rock matrix and tend to hide the so-called fluid effect (i.e. the effect of different fluid saturations on the elastic properties), thus making the discrimination between different saturation conditions more and more problematic.

I start by presenting the theoretical background used to derive the linear petrophysical-AVA forward operators. Then, the theoretical aspects of sensitivity analysis and AVA-petrophysical inversion are discussed. I move on by describing and validating the different RPMs derived for the considered reservoir. Then, I perform the AVA-petrophysical inversion of the analytical *Rpp* responses derived from logged elastic properties, and I theoretically investigate the results provided by this inversion procedure. In the last section the effects of different elastic parameterizations on litho-fluid facies identification are discussed.

2. Elastic AVA forward modelling and the AVA-petrophysical inversion

In the following discussion, the vector **r** represents the petrophysical properties of interest [water saturation, *Sw*; porosity, ϕ; shaliness, *Sh*; $\mathbf{r} = (Sw, \phi, Sh)^T$], whereas **m** indicates the natural logarithm of a triad of elastic properties {i.e., $\mathbf{m} = [\ln(Vp), \ln(Vs), \ln(\rho)]^T$} that is, in turn, associated with a given elastic parameterization. Finally, the vector **d** contains the analytical *Rpp* responses derived by applying the petrophysical-AVA forward operators to logged elastic parameters. As previously discussed, many linear approximations of the full Zoeppritz (1919) equations exist. In this paper, I analyse four among the most popular:

$$Rpp(\theta) = \left(\frac{1}{2\cos^2(\theta)}\right)\frac{\Delta I_p}{\overline{Ip}} - 4\left(\frac{\overline{Is^2}}{\overline{Ip^2}}\sin^2(\theta)\right)\frac{\Delta Is}{\overline{Is}} + \left(\frac{1}{2} - \frac{1}{2\cos^2(\theta)} + 2\frac{\overline{Is^2}}{\overline{Ip^2}}\sin^2(\theta)\right)\frac{\Delta\rho}{\bar{\rho}} \quad (1)$$

$$Rpp(\theta) = \frac{1}{2}(1 + tan^2(\theta))\frac{\Delta Vp}{\overline{Vp}} - 4\left(\frac{\overline{Vs^2}}{\overline{Vp^2}}\sin^2(\theta)\right)\frac{\Delta Vs}{\overline{Vs}} + \frac{1}{2}\left(1 - 4\frac{\overline{Vs^2}}{Vp^2}\sin^2(\theta)\right)\frac{\Delta\rho}{\bar{\rho}} \quad (2)$$

$$Rpp(\theta) = \left(\frac{1}{4} - \frac{1}{2}\frac{\overline{Vs^2}}{\overline{Vp^2}}\right)sec^2(\theta)\frac{\Delta(\lambda\rho)}{\overline{\lambda\rho}} - \left(\frac{1}{2}sec^2(\theta) - 2sin^2(\theta)\right)\frac{\overline{Vs^2}}{\overline{Vp^2}}\frac{\Delta(\mu\rho)}{\overline{\mu\rho}} + \frac{1}{2}\left(\tan^2(\theta) - 4\frac{\overline{Vs^2}}{\overline{Vp^2}}sin^2(\theta)\right)\frac{\Delta\rho}{\bar{\rho}} \quad (3)$$

$$Rpp(\theta) = \frac{1}{4}\left(1 - 2\frac{\overline{Vs^2}}{\overline{Vp^2}}sec^2(\theta)\right)\frac{\Delta\lambda}{\bar{\lambda}} - \frac{1}{2}\left(\frac{\overline{Vs^2}}{\overline{Vp^2}}sec^2(\theta) - 4\sin^2(\theta)\right)\frac{\Delta\mu}{\bar{\mu}} + \frac{1}{2}\left(1 - \frac{1}{2}sec^2(\theta)\right)\frac{\Delta\rho}{\bar{\rho}} \tag{4}$$

where *Rpp* is the P-wave reflection coefficient, and θ represents the incidence angle. In Eq. 1, *Ip* indicates the P-wave impedance, *Is* the S-wave impedance, and ρ the density. In Eq. 2, *Vp* and *Vs* represent the P-wave and S-wave velocities, respectively, whereas in Eqs. 3 and 4, λ and μ are the first and second Lamé parameters, respectively. In Eqs. 1 to 4, Δx and $\bar{x}$ are the contrast and the average value of a given elastic property x across the reflecting interface, respectively. Eqs. 1 to 4 represent what I call the elastic-AVA forward modelling. In particular, Eqs. 1 and 2 are taken from Aki and Richards (1980); Eq. 3 was first defined by Goodway *et al.* (1997) and successively modified by Thomas *et al.* (2016). Finally, Eq. 4 was derived by Gray *et al.* (1999).

If we consider a weak contrast for the elastic property x at the reflecting interface, we can write (Stolt and Weglein, 1985):

$$\Delta \ln(x) \approx \frac{\Delta x}{\bar{x}} \tag{5}$$

This assumption enables us to rewrite Eqs. 1 to 4 in the following, more general, form:

$$Rpp(\theta) = \alpha_{x1}\Delta\ln(x_1) + \alpha_{x2}\Delta\ln(x_2) + \alpha_{x3}\Delta\ln(x_3) \tag{6}$$

where x_1, x_2, and x_3 identify a triad of elastic properties, whereas the α terms represent the influence of each elastic property on the P-wave reflection coefficients. For example, in Eq. 1 the three α terms are the following:

$$\alpha_{Ip}(\theta) = \frac{1}{2\cos^2(\theta)} \tag{7.1}$$

$$\alpha_{Is}(\theta) = -4\frac{\overline{Is}^2}{\overline{Ip}^2}\sin^2(\theta) \tag{7.2}$$

$$\alpha_{\rho}(\theta) = \left(\frac{1}{2} - \frac{1}{2\cos^2(\theta)} + 2\frac{\overline{Is}^2}{\overline{Ip}^2}\sin^2(\theta)\right) \tag{7.3}$$

Now I rewrite the reflectivity function of Eq. 6 in terms of petrophysical properties according to Aleardi *et al.* (2017a). First, a linear rock-physics model must be defined:

$$\ln(x) = a_1 + a_2\phi + a_3 Sw + a_4 Sh; \tag{8}$$

where x represents an elastic property, and a_1, a_2, a_3, and a_4 are the regression coefficients that can be determined by a linear regression procedure driven by well-log information pertaining to the investigated area. Differentiating Eq. 8 sample-by-sample, by applying the Δ operator, leads to:

$$\Delta\ln(x) + \alpha_2\Delta\phi + \alpha_3\Delta Sw + \alpha_4\Delta Sh; \tag{9}$$

With Eq. 9 the contrasts in the elastic properties are expressed in terms of contrasts in the petrophysical properties. Eq. 9 can be compactly written in matrix form as:

$$\mathbf{Dm = BDr} \tag{10}$$

where the matrix **B** contains the *a* coefficients of Eq. 9, and **D** is the differential matrix operator. By combining Eqs. 6 and 10 gives:

$$\mathbf{Rpp = ABDr = FDr = Gr} \tag{11}$$

where the matrix **A** contains the coefficients α_{x1}, α_{x2} and α_{x3} expressed, for instance, in Eqs. 7.1 to 7.3. By writing Eq. 11 in a form similar to that of Eqs. 1 to 4, leads to:

$$Rpp\,(\theta) = f_{\varphi}(\theta)\,\Delta\varphi + f_{Sw}(\theta)\Delta Sw + f_{Sh}(\theta)\,\Delta Sh \tag{12}$$

where f_{φ}, f_{Sw}, and f_{Sh} are the coefficients contained in the matrix **F** that express the influence of each petrophysical property in the P-wave reflection coefficients. Eqs. 11 and 12, respectively, represent the matrix and analytical expressions of the petrophysical-AVA forward modelling that can be derived for each considered elastic parameterization (Eqs. 1 to 4). Both the elastic- and petrophysical-AVA linear forward modellings can be analysed with the sensitivity analysis tools. The sensitivity analysis is a powerful approach to theoretically investigate the physical meaning of the forward modelling operators, and more importantly, for linear forward operators, the outcomes of this analysis are wholly independent from the data and only dependent on the mathematical properties of the forward operator (Menke, 2012). For example, the SVD decomposition of **G** can be expressed as:

$$\mathbf{G = USV^T} \tag{13}$$

where **S** is a diagonal matrix of singular values, **V** is the matrix of eigenvectors in the model space, and **U** contains the eigenvectors in the data space. The energy of each component is given by the corresponding eigenvalue. If the orders of magnitude of the eigenvalues are significantly different, a high signal-to-noise ratio is needed to estimate the signal in the low-energy directions. The SVD decomposition is essential in sensitivity analysis because it permits having a better understanding of the physical meaning of the forward modelling. Indeed, this decomposition allows the reflectivity *Rpp* to be divided into three orthogonal components in both data space and model space. The eigenvectors **V** are a basis in the model space. The eigenvalues **S** represent the reflected energy due to medium perturbations along the eigenvectors in the model space. The amplitude versus angle effects of the reflections are described by the eigenvectors in the data space (**U**), which are three orthogonal functions (De Nicolao *et al.*, 1993). To understand how an error in the data propagates as an error in the estimated model, it is useful to define the model covariance matrix $\mathbf{C_m}$. If the data are assumed to be uncorrelated and all have equal variance, the unit model covariance matrix is given by:

$$\mathbf{C_m = (G^TG)^{-1}} \tag{14}$$

The unit model covariance matrix is a measure of how uncorrelated noise with unit variance in the data is mapped into uncertainties in the estimated model parameters. The diagonal terms indicate the variance associated with each model parameter, whereas the off-diagonal terms indicate the covariances. In addition, the model covariance matrix is a function of only the data kernel (the **G** matrix) and of any a-priori information added to the problem.

In the AVA-petrophysical inversion I apply Eq. 11 to the logged *Vp*, *Vs*, and ρ values to estimate the analytical *Rpp* responses that are inverted to infer the petrophysical properties of interest. In particular, I exploit borehole information pertaining to different exploration wells to calibrate different RPMs that are then used to predict the petrophysical properties in a well not used in the calibration process. Obviously, in this blind test experiment I assume that the RPMs estimated at the well locations are also valid far away from the calibration wells. The inversion approach I apply follows the line of the Bayesian inversion algorithm proposed by Buland and Omre (2003). Being **G** the linear forward operator that links the *Rpp* response to the petrophysical properties (Eq. 11), if we assume a multivariate Gaussian a-priori probability density function (PDF) for **r** (i.e. a Gaussian marginal a-priori PDF for porosity, water saturation, and shaliness), and Gaussian distributed noise, the estimated petrophysical parameters are still represented by a multivariate Gaussian a-posteriori PDF $p(\mathbf{r}|\mathbf{d})$ with explicit expressions for the a-posteriori mean $\boldsymbol{\mu}_{(\mathbf{r}|\mathbf{d})}$ and covariance $\boldsymbol{\Sigma}_{(\mathbf{r}|\mathbf{d})}$:

$$\boldsymbol{\mu}_{(\mathbf{r}|\mathbf{d})} = \boldsymbol{\mu}_{\mathbf{r}} + \boldsymbol{\Sigma}_{\mathbf{r}}\mathbf{G}^{T} (\mathbf{G}\boldsymbol{\Sigma}_{\mathbf{r}}\mathbf{G}^{T} + \boldsymbol{\Sigma}_{\mathbf{e}})^{-1} (\mathbf{d}-\mathbf{G}\boldsymbol{\mu}_{\mathbf{r}}); \tag{15.1}$$

$$\boldsymbol{\Sigma}_{(\mathbf{r}|\mathbf{d})} = \boldsymbol{\Sigma}_{\mathbf{r}} - \boldsymbol{\Sigma}_{\mathbf{r}}\mathbf{G}^{T} (\mathbf{G}\boldsymbol{\Sigma}_{\mathbf{r}}\mathbf{G}^{T} + \boldsymbol{\Sigma}_{\mathbf{e}})^{-1} \mathbf{G}\boldsymbol{\Sigma}_{\mathbf{r}}; \tag{15.2}$$

where, $\boldsymbol{\mu}_{\mathbf{r}}$ and $\boldsymbol{\Sigma}_{\mathbf{r}}$ are the mean and the covariance of the a-priori distribution of **r** that can be derived from available well-log information, whereas $\boldsymbol{\Sigma}_{\mathbf{e}} = \boldsymbol{\Sigma}_{\mathbf{n}} + \boldsymbol{\Sigma}_{\mathbf{RPM}}$. The covariance matrix $\boldsymbol{\Sigma}_{\mathbf{n}}$ expresses the noise in the measured data, whereas the matrix $\boldsymbol{\Sigma}_{\mathbf{RPM}}$ defines the uncertainties affecting the considered RPM. Note that this formulation of the error covariance matrix allows properly propagating the uncertainties affecting the rock-physics models into the final petrophysical predictions. To this end, the differences between the logged elastic properties and the elastic properties predicted by the linear RPMs, are used to derive the matrix with an approach similar to that described in Aleardi *et al.* (2017b). I assume that this difference follows a Gaussian distribution with a covariance matrix $\boldsymbol{\Sigma}_{\varepsilon}$ and a null mean value $\boldsymbol{\mu}_{\varepsilon}$:

$$p(\boldsymbol{\varepsilon}) = N(\boldsymbol{\varepsilon};\boldsymbol{\mu}_{\varepsilon} = 0,\boldsymbol{\Sigma}_{\varepsilon}) \tag{16}$$

where *N* represents the Gaussian distribution. After defining the $p(\varepsilon)$ distribution, a Monte Carlo sampling algorithm can be used to derive the $\boldsymbol{\Sigma}_{\mathbf{RPM}}$ matrix.

To reduce the ill-conditioning of the petrophysical inverse problem, I include a-priori information about the vertical variability of petrophysical properties in the inversion. This information can be introduced into the a-priori covariance matrix $\boldsymbol{\Sigma}_{\mathbf{r}}$ that can be obtained by a Kronecker product between a stationary covariance matrix (expressing the mutual correlation of petrophysical properties), and a vertical correlation function that aims to reproduce the actual vertical variability of petrophysical properties. Both the stationary covariance matrix and the vertical variability of petrophysical properties can be derived from available borehole information.

Similarly to Buland and Omre (2003), I use a second-order exponential function to express the vertical correlation:

$$v_t(\tau;\xi_1;\xi_2) = \frac{1}{2}\exp\left[-\left(\frac{\tau}{\xi_1}\right)^2\right] + \frac{1}{2}\left(1-\frac{2\tau^2}{\xi_2^2}\right)\exp\left[-\left(\frac{\tau}{\xi_2}\right)^2\right] \quad (17)$$

where τ is the time-lag and, ξ_1 and ξ_2 are the parameters characterizing the temporal dependency.

3. Rock physics modelling

The reservoir considered in this study is located in gas-bearing sands at the depth range of 2300-2700 m (around 2400-2560 ms in seismic two-way-time) that pertain to the slope-channel systems of Plio-Pleistocene age in offshore Egypt. Borehole logs from different wells provide elastic and petrophysical information needed to fully characterize the reservoir rocks in terms of P- and S-wave velocities, density, effective porosity, water-saturation and shaliness (i.e. dry clay + clay-bound water). The reservoir consists of a sequence of three/four main sand layers interbedded with laminated non-permeable shales. The reservoir sand is fairly clean with negligible cementation and low clay content; available well-log data show that effective porosity ranges from 0 to 35%, while gas saturation varies between 0% and 80%. The layers above and below the reservoir mostly contain shale. Aleardi and Ciabarri (2017) showed that for the investigated reservoir, the relation linking the petrophysical properties to the elastic parameters can be conveniently described by a multilinear model that can be estimated using a stepwise regression approach. As concerns this study, I use the same regression algorithm to estimate the linear relations linking the natural logarithm of different elastic parameters to the petrophysical properties (see Eq. 8). This procedure has provided the following equations:

$$\ln(Vp) = 7.6908 - 0.0103\phi + 0.0020Sw - 0.0011Sh \quad (18.1)$$

$$\ln(Vs) = 7.4111 - 0.0174\phi - 0.0002Sw - 0.0056Sh \quad (18.2)$$

$$\ln(\rho) = 0.8291 - 0.0056\phi + 0.0013Sw - 0.0011Sh \quad (18.3)$$

$$\ln(Ip) = 8.4996 - 0.0157\phi + 0.0035Sw - 0.0027Sh \quad (18.4)$$

$$\ln(Is) = 8.2609 - 0.0232\phi + 0.0014Sw - 0.0071Sh \quad (18.5)$$

$$\ln(\lambda) = 14.8706 - 0.0174\phi + 0.0091Sw + 0.0024Sh \quad (18.6)$$

$$\ln(\mu) = 15.6560 - 0.0401\phi + 0.0013Sw - 0.0132Sh \quad (18.7)$$

$$\ln(\lambda\rho) = 15.7923 - 0.0265\phi + 0.0102Sw + 0.0013Sh \quad (18.8)$$

$$\ln(\mu\rho) = 16.5213 - 0.0462\phi + 0.0020Sw - 0.0143Sh \quad (18.9)$$

where Vp and Vs are expressed in m/s, ρ in g/cm^3, whereas Sw, φ and Sh in percentage (varying from 0% to 100% for Sw and Sh and from 0% to 35%, approximately, for φ). As an example, if we limit the focus on the coefficients associated to Vp, Vs, and ρ, we note that, as expected, these parameters decrease as the porosity increases (the φ parameter has always a negative coefficient);

the *Vp* and ρ increase as the water saturation increases since gas is characterized by a lower bulk modulus (and density) than water. Conversely, the shear modulus is not affected by the saturating fluid and this fact, together with the ρ decreasing caused by the increase in hydrocarbon saturation, explain the *Vs* increasing as the water saturation decreases. The negative coefficients associated to *Sh* can be related to the depth interval I consider (2300-2700 m), characterized by a mechanical compaction regime. In this depth interval, the *Vp*, *Vs* and ρ of shales are lower than those of sands as confirmed by a direct analysis of available well-log data (Aleardi and Ciabarri, 2017). Finally, note that in all the Eqs. 18.1 to 18.9, the magnitude of the coefficients decreases moving from porosity, to shaliness, and water saturation. Therefore, we can conclude that the porosity plays the major role in determining the elastic properties, whereas the other two petrophysical parameters exert weaker influences on such properties. From this consideration, I expect that the porosity will be the best resolved parameter in the AVA-petrophysical inversion, whereas shaliness and water saturation will be less resolved.

To better demonstrate the capability of the derived RPMs to express the actual relationships linking petrophysical and elastic properties in the investigated reservoir, I show in Fig. 1 comparisons between logged and predicted elastic properties by the linear RPMs. The good matches between actual and the predicted properties prove that the linear RPMs are effective approximations of the actual physical relationships linking elastic and petrophysical properties in the considered area.

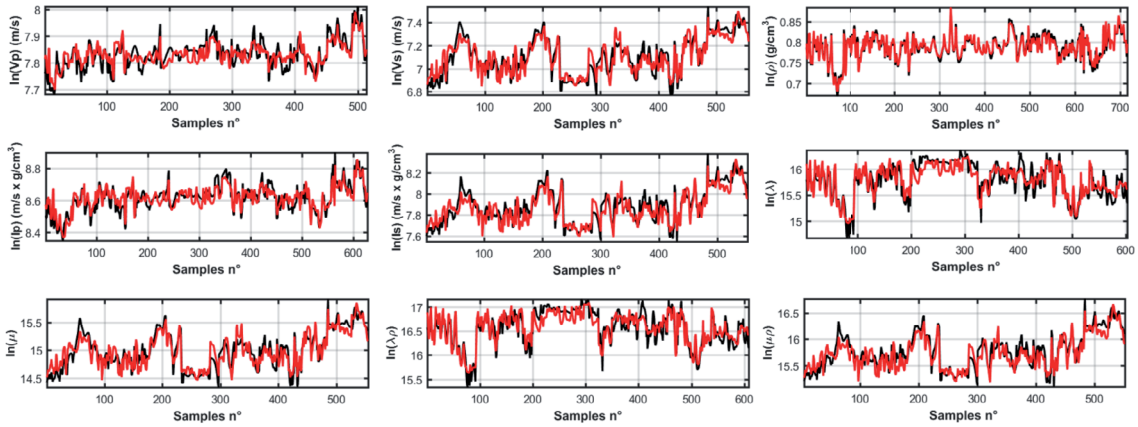

Fig. 1 - Comparison between actual (black lines) and predicted (red lines) elastic parameters by the linear RPMs of Eqs. 18.1 to 18.9. The parameters *Vp*, *Vs*, ρ, *Ip*, *Is*, λ, μ, $\lambda\rho$, and $\mu\rho$ are represented from top left to bottom right, respectively. Note that the predicted properties closely follow the true properties.

Fig. 2 shows the linear correlation coefficients between predicted and true elastic parameters. Note that all the correlation coefficients are higher than 0.8, thus indicating that the linear RPMs of Eqs. 18.1 to 18.9 provide good predictions. As expected, the highest correlation coefficient (around 0.98) is associated to the ρ parameter. Indeed, it is known that an almost linear relation links this elastic attribute to the petrophysical rock properties (Avseth *et al.*, 2005).

In Figs. 3 and 4, I represent two examples of rock-physics templates (RPTs) that allow a better assessment of the actual capabilities of the linear RPMs of reproducing the actual influence played by each petrophysical property in determining the elastic parameters. Note that the general

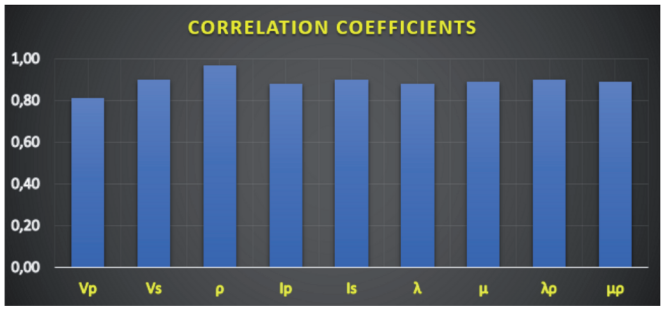

Fig. 2 - Linear correlation coefficients between true and predicted elastic parameters. Note that all the correlation coefficients are higher than 0.8 and that ρ gives a correlation coefficient around 0.98.

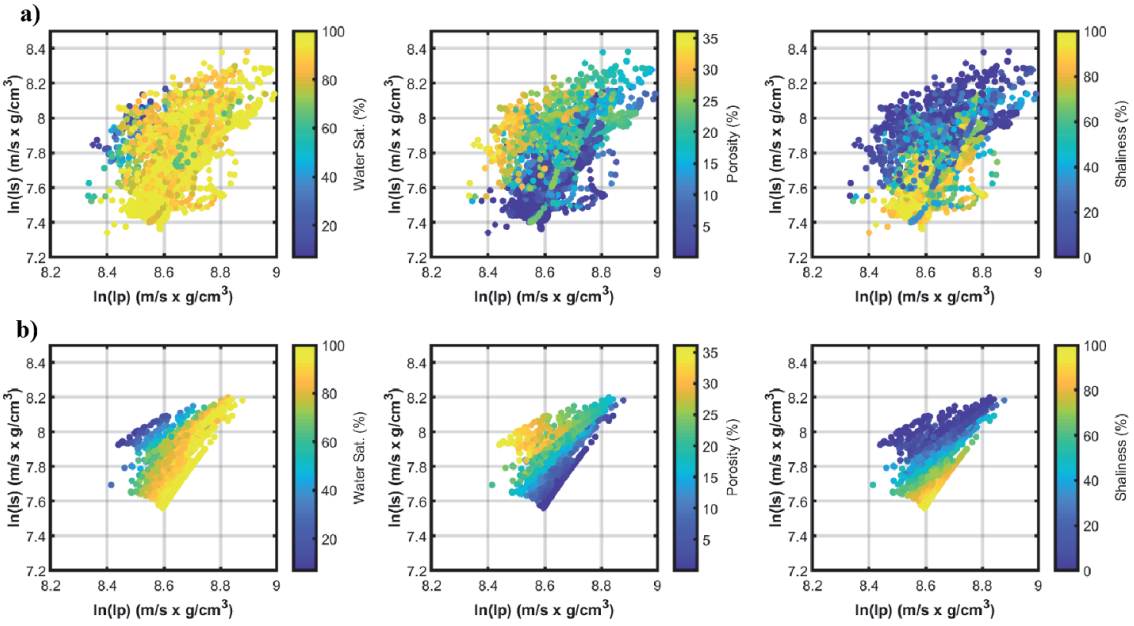

Fig. 3 - Comparison between actual and predicted RPTs. a) RPTs derived from actual well-log data and showing the influence of each petrophysical parameter on the natural logarithm of the P-impedance (*Ip*) and S-impedance (*Is*) values. The influence of water saturation, porosity, and shaliness is represented from left to right. b) RPTs predicted by the linear Eqs. 18.4 to 18.5. Note that the main trends visible in a) are well reproduced by the estimated RPMs.

trends derived from actual well-log data are closely matched by the RPTs derived from the linear RPMs. This result further proves the suitability of the estimated linear rock-physics equations for reservoir characterization in the investigated zone. Similar considerations would have been drawn by observing different RPTs (i.e. *Vp*-*Vs*, or λ-μ).

The differences between actual and predicted properties may obviously be ascribed to the inability of the linear RPMs to fully reproduce the influence played by each petrophysical property on the elastic parameters, and also to the intrinsic petrophysical heterogeneities of the investigated reservoir rocks (i.e. mineralogical heterogeneities). However, as previously described, these differences are accounted for in the AVA-petrophysical inversion and correctly propagated into the final predictions.

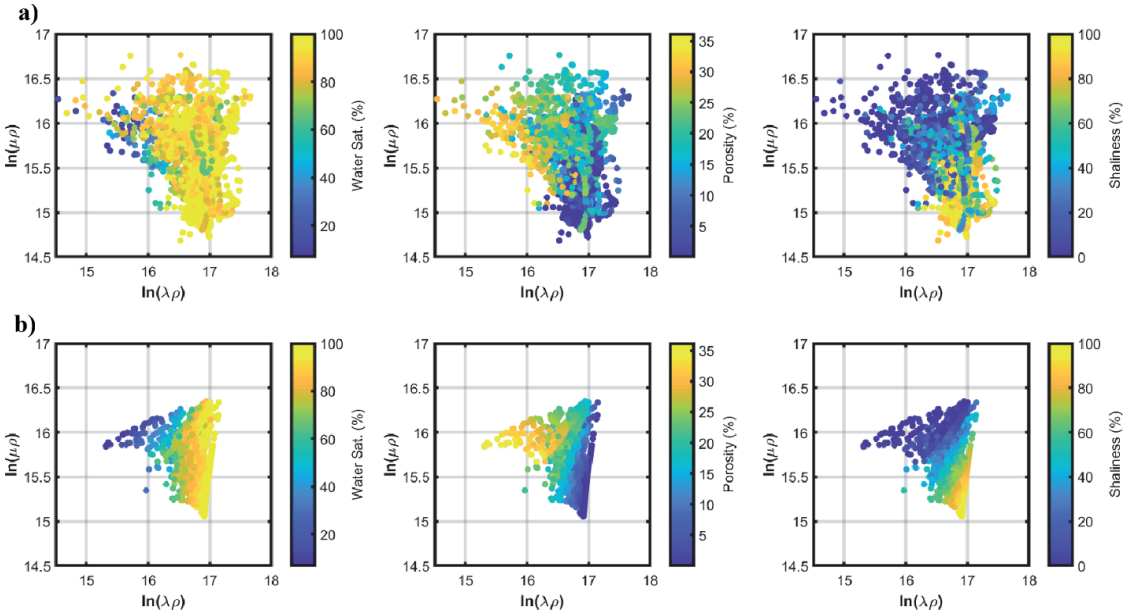

Fig. 4 - Comparison between actual and predicted RPTs. a) RPTs derived from actual well-log data and showing the influence of each petrophysical parameter on the natural logarithm of $\lambda\rho$ and $\mu\rho$. The influence of water saturation, porosity and shaliness is represented from left to right. b) RPTs predicted by the linear Eqs. 18.8 and 18.9. Note that the main trends visible in a) are well reproduced by the estimated RPMs.

4. Assessing the prediction capabilities of the derived linear RPMs and analysing the effects of different elastic parameterizations in AVA-petrophysical inversion

I now describe the results of the AVA-petrophysical inversion in which the derived petrophysical-AVA forward operators are used to estimate the petrophysical properties from the analytical *Rpp* responses derived from logged elastic properties. The aim of this section is two-fold. First, this inversion test performed on a blind well allows demonstrating the actual prediction capabilities of the linear RPMs. Secondly, this inversion enables rapidly checking the influence of the different elastic parameterizations (used to derive the four petrophysical-AVA forward modellings) in the predicted petrophysical properties and related uncertainties. Note that this inversion is performed at the well-log scale. Indeed, it inverts the analytical *Rpp* responses, and not the seismic data that can be obtained by convolving the *Rpp* series with a source wavelet. In this way, the additional source of uncertainties introduced by the different scale of well-log data (used to define the RPMs) and the seismic data, can be neglected (Grana and Della Rossa, 2010).

I apply Eq. 2 to the logged *Vp*, *Vs*, and ρ values to derive the analytical *Rpp* responses that constitutes the observed data (the vector **d** in Eqs. 15.1 to 15.2) for the AVA-petrophysical inversion. To better simulate a field dataset, I add Gaussian distributed random noise to the analytical *Rpp* responses by imposing a signal-to-noise (S/N) ratio equal to 10, where the S/N ratio is defined as the power of the signal divided by the power of the noise. The final results, which are the conditional PDFs of petrophysical properties given the *Rpp* responses $p(\mathbf{r}|\mathbf{d})$ obtained for each elastic parameterization, are displayed in Fig. 5. At a glance, we can observe that the different parameterizations yield very similar results for both the shape of the probability distributions and the maximum a posteriori (MAP) solutions. These results are consistent with the true property

values and correctly capture the variability in the logs. As expected, the water saturation and the shaliness parameters are always less resolved than porosity. The results shown in Fig. 5 clearly demonstrate the reliability and prediction capability of the derived RPMs.

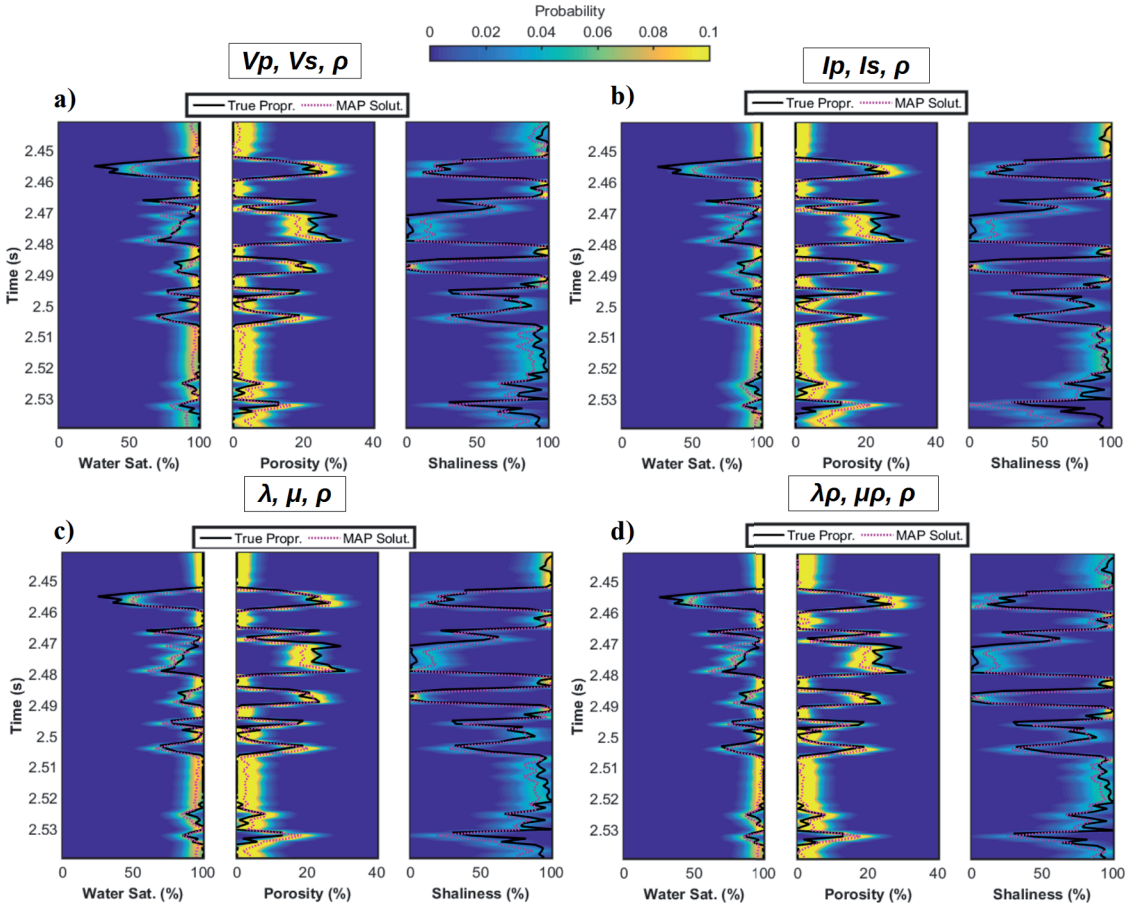

Fig. 5 - Results of the AVA-petrophysical inversions in which analytical *Rpp* responses are inverted by considering the four petrophysical-AVA forward modellings: a), b), c), and d) represent the results for the *Vp-Vs-ρ*, *Ip-Is-ρ*, *λ-μ-ρ*, and *λρ-μρ-ρ* parameterizations, respectively. The black solid lines represent the true logged property values, whereas the dotted magenta lines show the MAP solutions resulting from the AVA-petrophysical inversion. In all cases water saturation, porosity, and shaliness are indicated from left to right. The linear colour scale codes the probability values.

For a more quantitative analysis of the results displayed in Fig. 5, I first compute the root-mean-square-error (RMSE) between the actual petrophysical property values and the MAP solutions estimated by each petrophysical-AVA forward operator. Fig. 6 demonstrates that the four elastic parameterizations give very similar RMSE values. In all cases, the porosity is the parameter affected by the lowest prediction error, whereas the water saturation and the shaliness estimates are less accurate. To quantitatively compare the posterior PDFs provided by each petrophysical-AVA forward operator, I compute the coverage probability that represents the actual probability that a given confidence interval contains the true property value. In the following I consider the 90% probability interval centred around the MAP solutions, and I compute the probability that this interval contains the true petrophysical values. Again, the different elastic parameterizations achieve very similar predictions, and as expected the porosity is the best determined parameter, followed by shaliness and water saturation (Fig. 7).

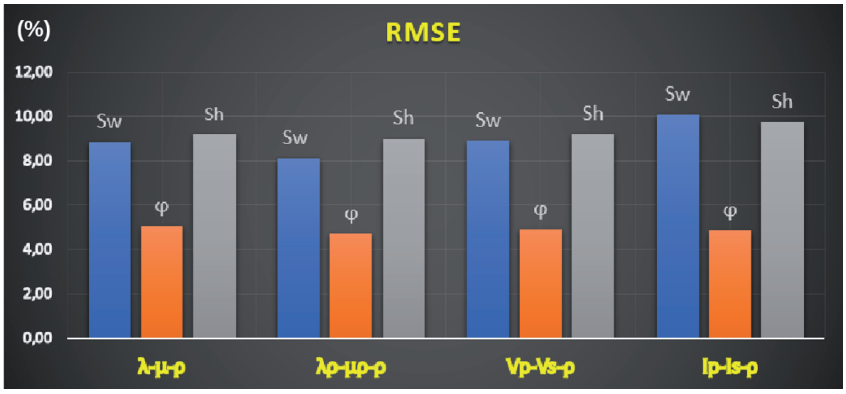

Fig. 6 - RMSE between the MAP solutions estimated by each petrophysical-AVA forward operator and the actual petrophysical property values. Note that the four forward operators give similar RMSE values for similar petrophysical properties.

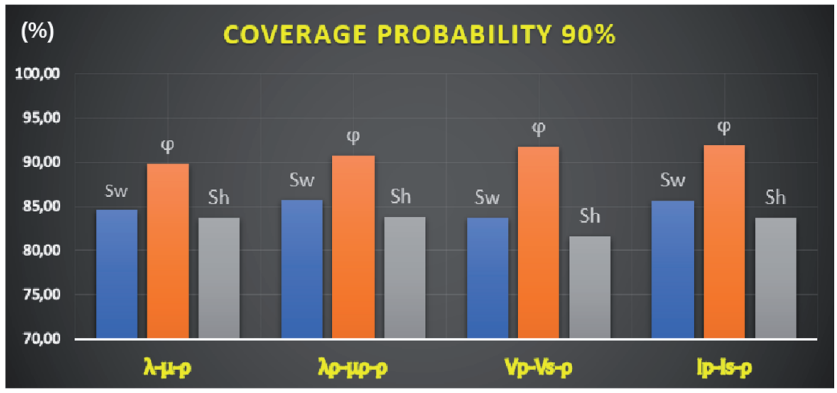

Fig. 7 - The coverage probability (90%) computed by considering the conditional PDF $p(\mathbf{r}|\mathbf{d})$ estimated by each petrophysical-AVA forward operator. Again, note the similarity of the results provided by each forward modelling.

5. Sensitivity analysis of the elastic- and petrophysical-AVA forward operators

I now theoretically investigate the results provided by the AVA-petrophysical inversion discussed in the previous section. Fig. 8 displays the eigenvectors in the model space derived for each considered elastic-AVA forward modelling and computed as the maximum incidence angle increases. By examining Fig. 8a, it can be seen that the Vp and ρ components are very similar for low angles in the first eigenvector. Therefore, this vector primarily points toward the direction of P-impedance perturbations. This result is obvious; the normal incidence reflection coefficient only depends on the acoustic impedance contrast. For high incidence angles, as the critical angle is approached, the ρ term decreases, while the Vp component strongly increases. This fact can be explained by considering that only the Vp parameter determines the critical angle of P-wave reflection coefficients. The influence of Vs on the first eigenvector is null over the entire angle range considered. The physical meanings of the second and third eigenvectors for low incidence angles are more difficult to interpret because they depend on combinations of different

perturbations. However, for high incidence angles (beyond 30°) the second and third eigenvectors rotate toward the ρ and the *Vs* directions, respectively. Also, note the cross-talk between the *Vp* and ρ (visible in the first and second eigenvectors) that makes an independent estimation of these two parameters impossible for a conventional AVA inversion limited to a narrow-angle range (Aleardi and Tognarelli, 2016). The direct comparison of Figs. 8a and 8b explains why Debski and Tarantola (1995) recommended using the *Ip-Is-*ρ parameterization instead of the *Vp-Vs-*ρ one. Indeed, Fig. 8b shows that the *Ip-Is-*ρ triad forms an orthonormal basis in the elastic parameter space: the first eigenvector points entirely toward the *Ip* perturbations over the whole angle range considered. Similarly, the second and third eigenvectors entirely point toward the *Is* and ρ parameters, respectively. Therefore, compared with the *Vp-Vs-*ρ parameterization, the *Ip-Is-*ρ triad minimizes the cross-talk between the elastic properties. Roughly speaking, the *Ip-Is-*ρ parameterization is a better choice than the *Vp-Vs-*ρ because it results in an almost diagonal model covariance matrix. If we consider the *Ip-Is-*ρ parameterization we may conclude that the *Ip* will be the best resolved parameter because it can be entirely estimated from the first eigenvector and associated singular value. The *Is* will be the second best resolvable parameter that is mainly estimated from the second eigenvector and associated singular value. Finally, ρ will be poorly resolvable because it only influences the third eigenvector. Figs. 8c and 8d display the eigenvectors associated to the λ-μ-ρ and $\lambda\rho$-$\mu\rho$-ρ parameterizations, respectively. These two parameterizations show a cross-talk similar to that analyzed in Fig. 8a. Therefore, from the elastic inversion point of view, these parameterizations represent bad choices because they make an independent estimation of elastic parameters impossible.

Fig. 9 represents the eigenvectors in the model space derived for each considered petrophysical-AVA forward modelling and computed as the maximum incidence angle increases. Note that the four petrophysical-AVA forward modellings, produce very similar eigenvector components. In particular, in all cases the first eigenvector points toward the porosity perturbations, whereas the second and the third point toward an intermediate direction between shaliness and water saturation. Therefore, I expect that the porosity is the best resolvable parameter, whereas the shaliness and the water saturation will be less resolvable. From the eigenvector analysis it emerges that the AVA-petrophysical inversion is completely uninfluenced by the different elastic parameterizations used to derive the petrophysical-AVA forward operators.

The perfect equivalence between the different elastic parameterizations in the AVA-petrophysical inversion is further confirmed by Fig. 10. In this case, we observe that different elastic parameterizations produce unit model covariance matrices in the petrophysical space with negligible differences. In particular, this figure further confirms that the error mainly affects the shaliness and the water saturation estimates, whereas the porosity proved to be the best resolved parameter. In other words, the inverted porosity values will be affected by minor uncertainties than the other two petrophysical properties. In addition, note that the off-diagonal terms that indicate the covariances between the petrophysical properties (that in other terms is the cross-talk between petrophysical properties), remain more or less constant for different petrophysical-AVA forward modellings. Following the considerations drawn by Debski and Tarantola (1995), I can claim that in the analyzed case there is no preferable elastic parameterization, because different parameterizations yield equivalent eigenvector components and unit model covariance matrices in the petrophysical space. I remark that different rock-physics models (i.e. derived for a different exploration target) could lead to different results.

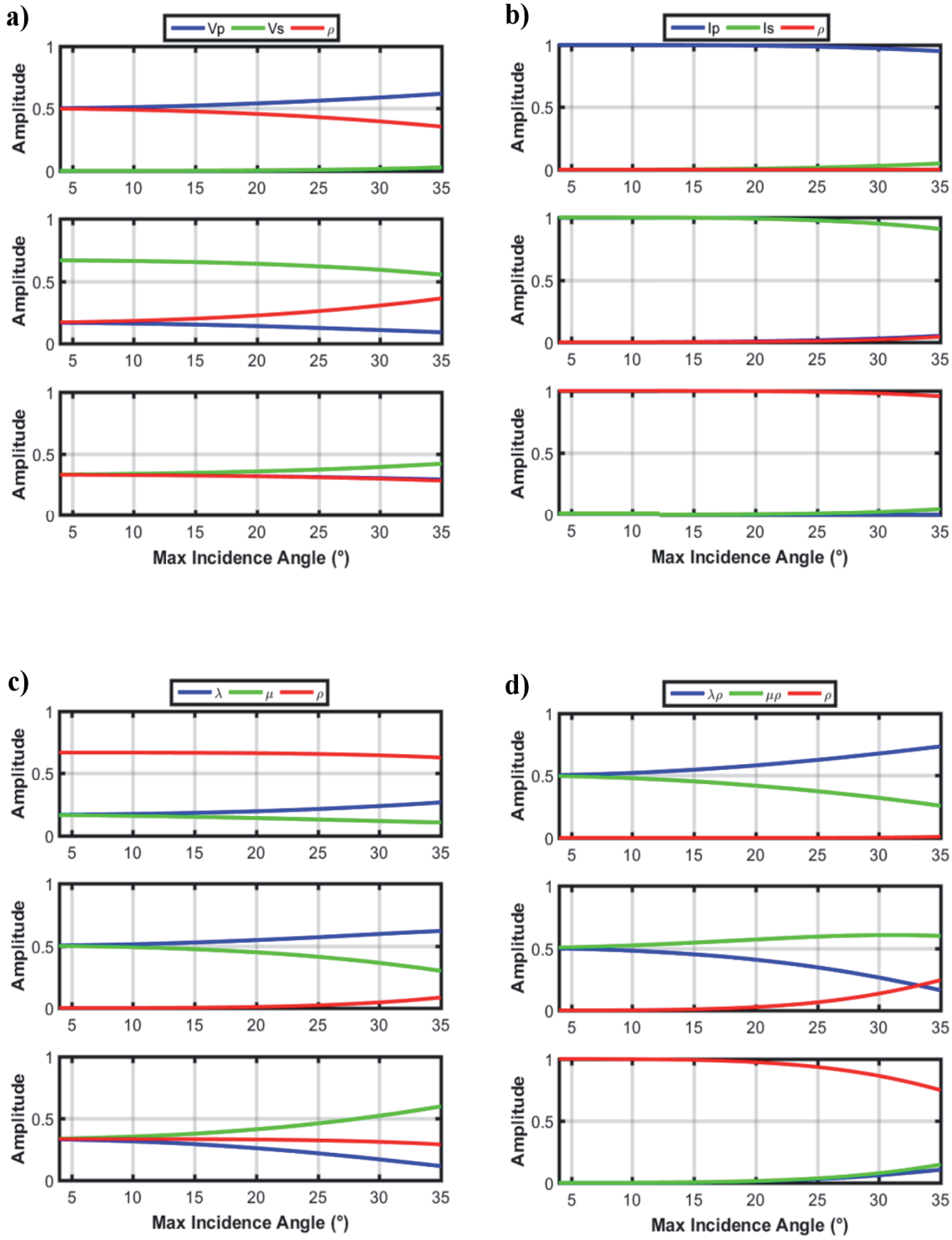

Fig. 8 - Eigenvectors in model space versus the maximum incidence angle, derived for the elastic-AVA forward modellings: a), b), c), and d) refer to the *Vp-Vs-ρ*, *Ip-Is-ρ*, *λ-μ-ρ*, and *λρ-μρ-ρ* parameterizations, respectively. In a), b), c), and d) the components of the first, second and third eigenvectors are represented from top to bottom, respectively.

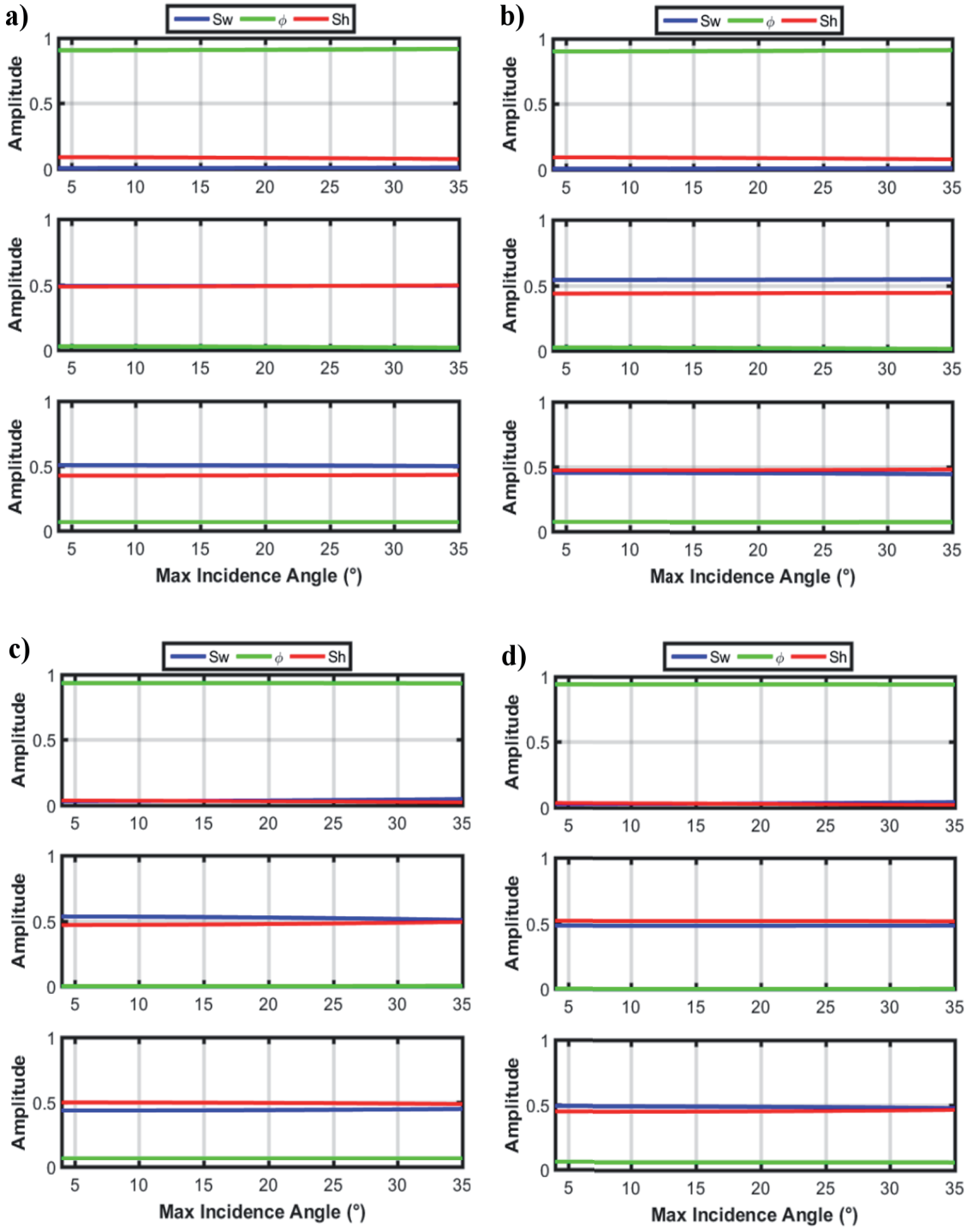

Fig. 9 - Eigenvectors in model space versus the maximum incidence angle, derived for the petrophysical-AVA forward modellings: a), b), c) and d) refer to the petrophysical forward modelling derived from the *Vp-Vs-ρ*, *Ip-Is-ρ*, *λ-μ-ρ*, and *λρ-μρ-ρ* parameterizations, respectively. In a), b), c), and d) the components of the first, second and third eigenvectors are represented from top to bottom, respectively. Note that the different petrophysical-AVA forward modellings are characterized by very similar eigenvector components.

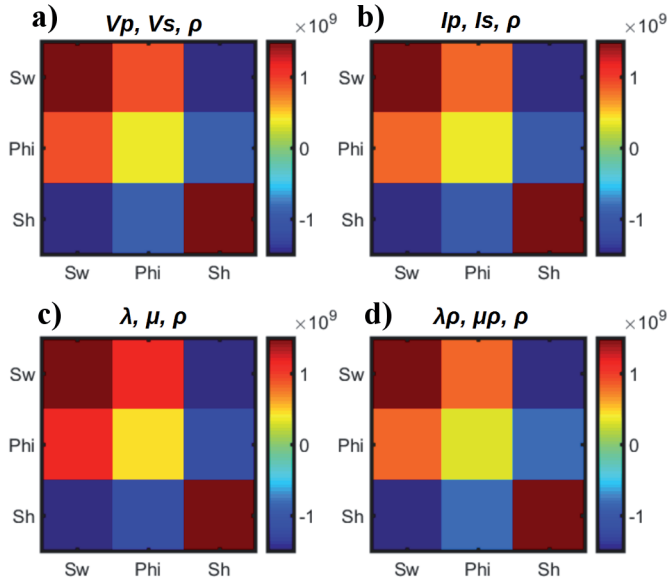

Fig. 10 - Unit model covariance matrices in the petrophysical space associated with the four petrophysical-AVA forward modellings. a), b), c), and d) refer to the petrophysical forward modelling resulting from the *Vp*-*Vs*-ρ, *Ip*-*Is*-ρ, λ-μ-ρ, and $\lambda\rho$-$\mu\rho$-ρ parameterizations, respectively. Note the close similarity between the covariance matrices associated to the different forward operators.

6. The effects of different elastic parameterizations in litho-fluid facies identification

In this second part, I discuss the results obtained in litho-fluid facies classification when different elastic parameterizations are considered. In this case, the classification procedure is directly performed on the logged elastic properties. In this way, and similarly to the AVA-petrophysical inversion, the additional uncertainties and resolution issues resulting from an elastic inversion of reflection seismic data can be neglected. The well-log data pertaining to the same blind well previously considered in the AVA petrophysical inversion, are the input to the classification procedure. In particular, a triad of elastic properties associated to a given elastic parameterization constitutes the input of the classification algorithm. Similarly to the AVA-petrophysical inversion, the logged *Vp*, *Vs*, and ρ values have been used to derive the other elastic properties: seismic impedances and Lamé parameters. The method I use to classify the elastic properties is the quadratic discriminant analysis that is briefly introduced in the following section.

7. Discriminant analysis

Linear or quadratic discriminant analysis is a deterministic method frequently used in pattern recognition or machine learning to separate a set of data in different classes or categories according to a set of measured properties or attributes. This method assumes that the input properties of each class follow a Gaussian distribution and uses a training data set to define the statistical characteristics (in terms of mean vector and covariance matrix) of this distribution. Being the

statistical model Gaussian within each facies, the resulting distribution is a Gaussian mixture that is a linear combination of Gaussian distributions. In case of linear discriminant analysis, the covariance matrices for all the classes are assumed to be identical, whereas quadratic discriminant analysis considers a different covariance matrix for each class. It results that when the covariance matrices are identical, the discriminant surfaces in the feature space are linear, whereas they become quadratic if the covariance matrices differ for the different classes.

In this work, I use the quadratic discriminant analysis and I classify each log sample on the basis of the Mahalanobis distance that in this case can be expressed as follows:

$$\mathbf{d}_z^{\pi} = (\mathbf{e}_i - \boldsymbol{\mu}_e^{\pi})^T (\boldsymbol{\Sigma}_e^{\pi})^{-1} (\mathbf{e}_i - \boldsymbol{\mu}_e^{\pi}) \tag{19}$$

where $\mathbf{e}$ is the vector containing the input samples to be classified that is a triad of elastic properties associated to a given elastic parameterization extracted from the blind well. The z term represents a given vertical position, whereas $\boldsymbol{\mu}_e$ and $\boldsymbol{\Sigma}_e$ are the mean vector and covariance matrix of the elastic properties in each litho-fluid facies. Finally, the superscript π indicates that these statistical properties are facies dependent. In this case $\boldsymbol{\mu}_e$ and $\boldsymbol{\Sigma}_e$ and are computed on a training data set constituted by the same well-log data previously used to calibrate the RPMs. After determining the $\mathbf{d}_z^{\pi}$ values for each input sample, this is classified into the litho-fluid class resulting in the minimum Mahalanobis distance. Application of the Mahalanobis distance to litho-fluid facies classification can be found in Mukerji *et al.* (2001), Avseth and Mukerji (2002), Avseth *et al.* (2005), and Del Monte *et al.* (2011).

8. The classification results

As previously introduced, three different facies are considered in the classification procedure: shale, brine sand, and gas sand. This choice was dictated by a priori knowledge about the investigated area derived from preliminary geologic interpretations integrated with core or well-log data. Fig. 11 shows four cross-plots representing the distribution of elastic properties within the three considered litho-fluid classes. The data used for this analysis have been extracted from the available borehole data around the reservoir zone. For conciseness, only a 2D map has been represented for each elastic parameterization. Let us focus on Fig. 11b representing the *Ip*-*Is* distribution. Note that the *Ip* progressively decreases passing from shale to brine sand and to gas sand. The lower *Ip* value for the gas sand with respect to the brine sand, is related to the decrease in bulk modulus that occurs when gas replaces brine in the pore space. Conversely, passing from shale to sands the *Is* increases due to the higher shear modulus that characterizes the sands with respect to shales. If we limit the attention to the S-impedance values, we note that the average *Is* values for brine and gas sands are very similar. This characteristic is related to the minor density variations that occur in the investigated, tight, reservoir sands when gas replaces brine in the pore space, and to the null effect played by the saturating fluid on the shear modulus. These two processes determine that the net *Is* value remains constant when passing from total brine to gas saturation. The different *Ip* and *Is* values of the shale with respect to the sand can obviously be ascribed to the different mineralogical compositions and geometric texture, whereas the significant overlap that characterizes the distribution of *Ip* and *Is* for gas sand and brine sands

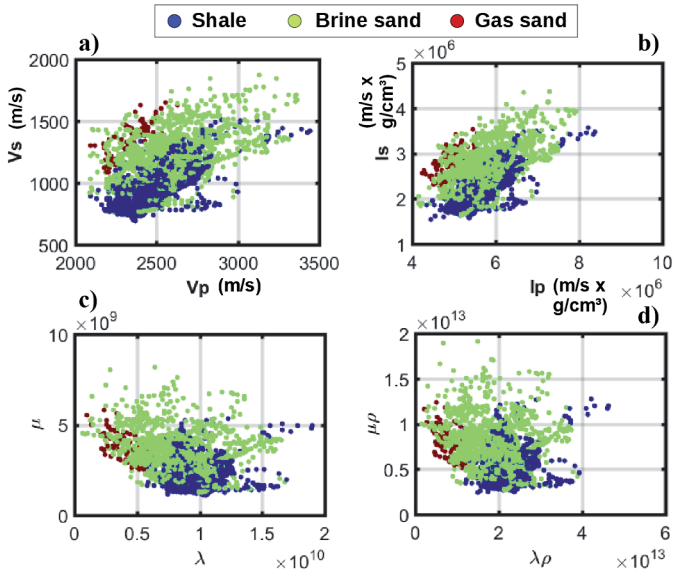

Fig. 11 - Cross-plots representing the distribution of different elastic properties within each considered litho-fluid facies. Note that independently of the considered pair of elastic properties, the three facies significantly overlap. In particular, the brine sand significantly overlaps the gas sand.

can be ascribed to the depth range in which the reservoir is located. Indeed, it is well known (Avseth *et al.*, 2003) that the increasing of burial depth tends to mask the fluid effect, and makes the discrimination between different saturation conditions more problematic. For this reason, the case under examination can be considered a challenging test for any classification method that aims to identify litho-fluid facies from elastic attributes.

If we shift attention to the other cross-plots of Fig. 11 we can observe that the overlaps between the elastic characteristics of the three facies persists. Differently from other well documented applications [e.g. Goodway *et al*. (1997), see introduction for details], in the investigated reservoir the different facies are not better discernible in different elastic domains (such as the $\lambda\rho$-$\mu\rho$ or λ-μ). Therefore, from a first qualitative analysis of Fig. 11, I can deduce that for the analysed reservoir the different elastic parameterizations will produce very similar predictions of litho-fluid facies.

In Fig. 12 I represent the Gaussian mixture distributions derived from the cross-plots of Fig. 11 by assuming Gaussian distributed properties within each litho-fluid class. Fig. 12 further confirms that the significant overlap between the different facies persists in different elastic domains. In particular, both the 2D and 1D probability distributions demonstrate that the elastic properties of brine sand are always significantly overlapped with those of gas sand and shale.

Figs. 13a and 13b, 14a and 14b, Fig. 15a and 15b, and 16a and 16b compare the 1D actual (derived from borehole information) and predicted vertical facies profiles for the blind well, when different elastic parameterizations are considered. Just the simple comparisons of the four predicted profiles confirm the considerations drawn from the cross-plot analysis. However, a more quantitative assessment of the outcomes of the classification procedure can be obtained by means of the contingency analysis tools (reconstruction rate, recognition rate, and estimation index; Figs. 13c to 13e, 14c to 14e, Fig. 15c to 15e, and 16c to 16e). The reconstruction rate represents the percentage of samples belonging to a litho-fluid class (actual), which are classified in that class (predicted). The recognition rate represents the percentage of samples classified in a litho-fluid class (predicted)

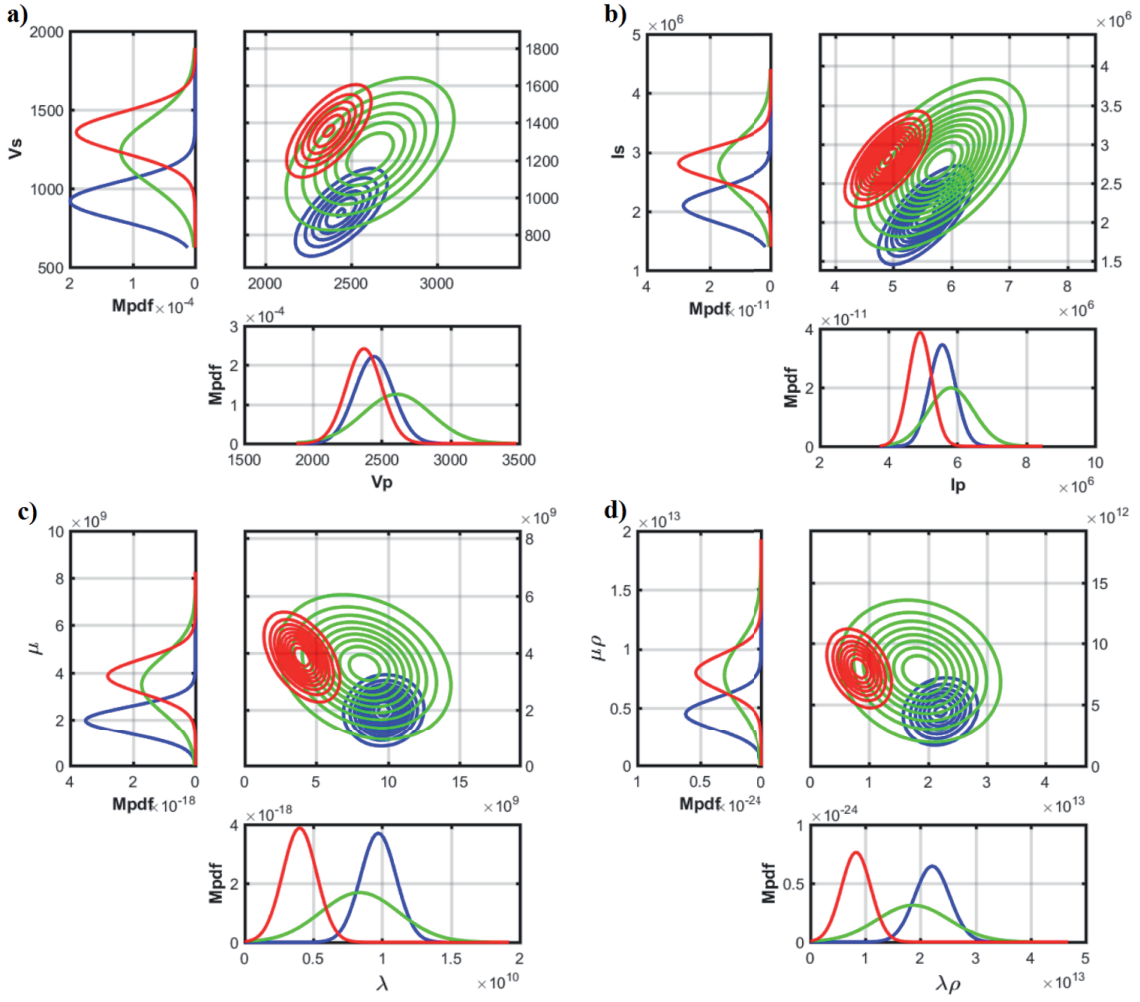

Fig. 12 - From a) to d) I represent the resulting Gaussian mixture distributions derived for each elastic parameterization from the cross-plots of Fig. 11. For each elastic parameterization I show the 3D Gaussian mixture distribution projected onto a 2D plane (*Vp-Vs*, *Ip-Is*, λ-μ, and $\lambda\rho$-$\mu\rho$ from panel a to d, respectively), together with the corresponding 1D marginal probability density functions (Mpdfs). Blue, green, and red colors represent shale, brine sand, and gas sand, respectively.

that actually belongs to that class (actual). Information concerning under/overestimation can be inferred from the estimation index that is defined as the difference between the reconstruction rate and recognition rate. A negative estimation index in the main diagonal indicates underestimation, and a positive estimation index indicates overestimation; the off-diagonal terms describe in which class the samples are misclassified. Figs. 13c to 13e, 14c to 14e, Fig. 15c to 15e, and 16c to 16e demonstrate that all the different elastic parameterizations yield overpredictions of brine sand and underpredictions of gas saturated sands. In particular, many gas sand and shale intervals are erroneously attributed to brine sands. The very similar results obtained for each considered elastic parameterization confirm that, for the investigated reservoir, there is no preferable triad of elastic parameters to be used for litho-fluid facies classification. This conclusion further demonstrates that the considerable depth at which the target reservoir is located makes a reliable facies classification particularly problematic whatever elastic parameterization is considered.

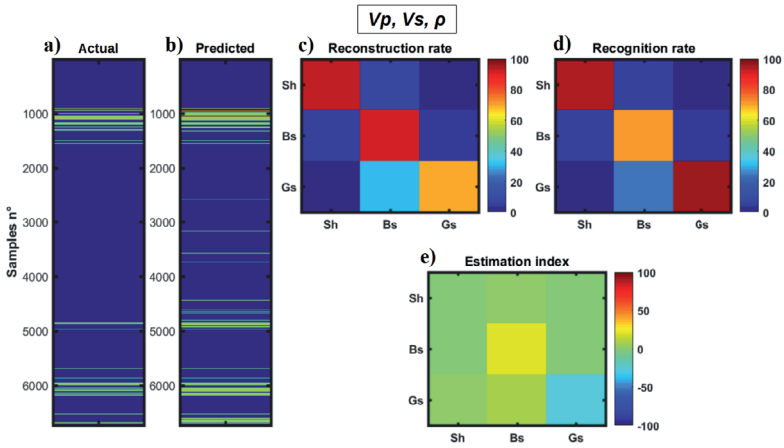

Fig. 13 - Actual (a) and predicted (b) vertical facies profiles obtained with the quadratic discriminant analysis when considering the *Vp-Vs-ρ* parameterization. Reconstruction rate (c), recognition rate (d) and estimation index (e) derived from a) and b). In a) and b) blue, green, and red represent shale, brine sand, and gas sand, respectively. In c), d), and e) Sh, Bs and Gs indicates shale, brine sand, and gas sand, respectively.

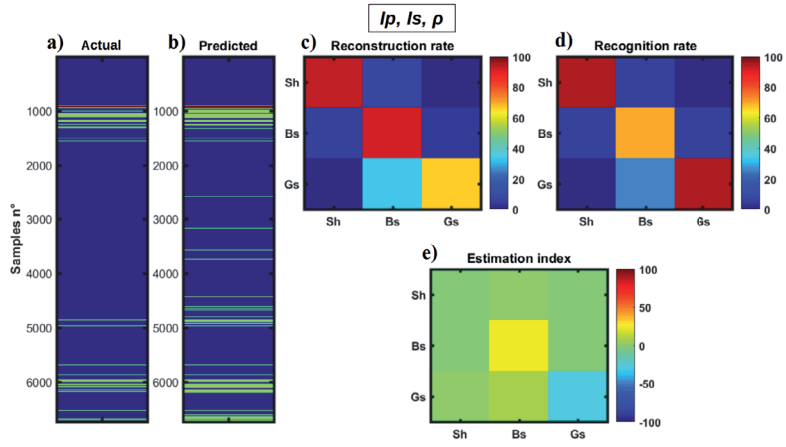

Fig. 14 - As in Fig. 13 but for the *Ip-Is-ρ* parameterization.

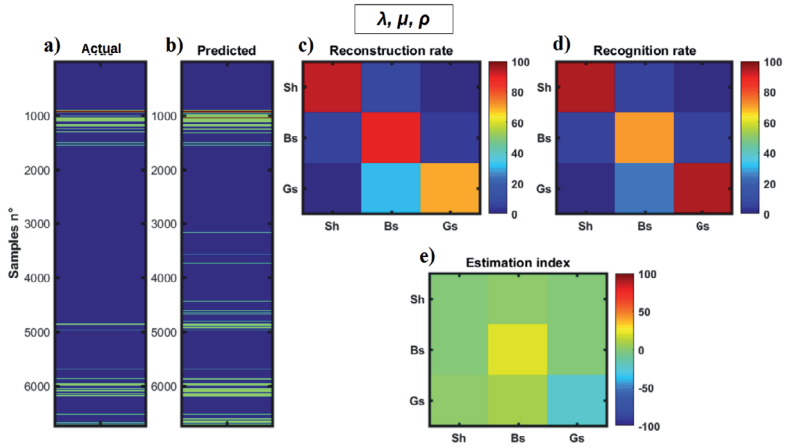

Fig. 15 - As in Fig. 13 but for the *λ-μ-ρ* parameterization.

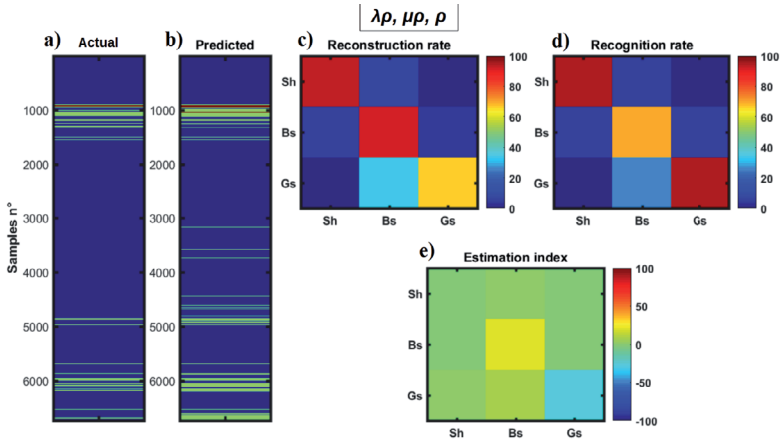

Fig. 16 As in Fig. 13 but for the $\lambda\rho$-$\mu\rho$-ρ parameterization.

8. Conclusions

I studied the effects of different elastic parameterizations in the AVA-petrophysical inversion and in the litho-fluid facies classification. I focused the analysis on a gas saturated reservoir located in offshore Egypt. The deep depth interval at which the reservoir zone is located (2300-2700 m) produces significant overlaps between the elastic properties of each facies. In particular, such significant depth interval stiffens the rock matrix and tends to partially hide the fluid effect, thus making the discrimination between different saturation conditions particularly problematic.

Regarding the AVA-petrophysical inversion, I considered four of the most popular linear approximations of the full Zoeppritz (1919) equations that link different triads of elastic properties to the P-wave reflection coefficients. Different linear, empirical rock-physics models have been derived for each considered elastic property by means of a multilinear stepwise regression driven by available well-log data. These linear rock-physics models enabled deriving four petrophysical-AVA forward operators, each one resulting from an elastic-AVA forward modelling. The AVA-petrophysical inversions performed on a blind well, demonstrated the reliability and the prediction capability of the linear RPMs, and also showed that the different elastic parameterizations exert a negligible influence on the outcomes of AVA-petrophysical inversion. To theoretically demonstrate this result, I performed a sensitivity analysis of the petrophysical-AVA forward operators. With regard to the resolvability of the petrophysical parameters and the error propagation from the data space to the petrophysical space, the sensitivity analysis confirmed that, for the investigated reservoir, the different elastic parameterizations do not influence the AVA-petrophysical inversion. In particular, it emerged that independently of the considered elastic parameterization, the porosity is the best resolved parameter, whereas the shaliness and the water saturations are less resolvable. The previous considerations have been drawn by considering linear RPMs specifically calibrated for the investigated reservoir area. However, rock-physics models are generally non-linear, but the nonlinearity is often not strong as in the reservoir zone considered in this work. In this context, the main advantages of considering linear RPMs consist in the analytical solutions of the Bayesian inverse problem, and in the independency of the sensitivity analysis results from the observed data. If necessary, a truncated Taylor series and an analytical derivation of the Jacobian

matrix could be used in case of slightly non-linear RPMs (i.e. Raymer model, stiff sand model, inclusion model) (Lang and Grana, 2017).

The litho-fluid facies classification performed on different triads of elastic properties, confirmed that the significant depth interval where the reservoir is located, makes distinguishing between the different litho-fluid facies (shale, brine sand and gas sand) particularly challenging. The contingency analysis of the classification results proved that for the investigated reservoir, differently from other well documented exploration targets, alternative elastic parameterizations (such as the $\lambda\rho$-$\mu\rho$) are not able to provide better discriminations between different litho-fluid facies. Therefore, I demonstrated that there is no preferable elastic parameterization for the litho-fluid facies identification in the target area.

As a final remark, I point out that the conclusions I draw are closely related to the investigated reservoir. For this reason, different geologic scenarios, characterized by different rock-physics models and different distributions of elastic properties within each litho-fluid facies, could lead to different conclusions.

Acknowledgments. The author wishes to thank Edison for the permission to publish this work and Fabio Ciabarri of Edison for the continuous support for this research project.

REFERENCES

Aki K. and Richards P.G.; 1980: *Quantitative seismology: theory and methods*. Freeman, San Francisco, CA, USA, Vol. I-II, 557-373 pp.

Aleardi M. and Ciabarri F.; 2017: *Assessment of different approaches to rock-physics modeling: a case study from offshore Nile Delta*. Geophys., **82**, MR15-MR25.

Aleardi M. and Mazzotti A.; 2017: *1D elastic full-waveform inversion and uncertainty estimation by means of a hybrid genetic algorithm - Gibbs sampler approach*. Geophys. Prospect., **65**, 64-85.

Aleardi M. and Tognarelli A.; 2016: *The limits of narrow and wide-angle AVA inversions for high Vp/Vs ratios: an application to elastic seabed characterization*. J. Appl. Geophys., **131**, 54-68.

Aleardi M., Ciabarri F., Gukov T., Giussani M. and Mazzotti A.; 2017a: *A single-step Bayesian petrophysical inversion algorithm based on a petrophysical reformulation of the P-wave reflection coefficients*. In: 79th EAGE Conf. and Exhib., Extended Abstracts, Paris, France, doi:10.3997/2214-4609.201700902.

Aleardi M., Ciabarri F. and Mazzotti A.; 2017b: *Probabilistic estimation of reservoir properties by means of wide-angle AVA inversion and a petrophysical reformulation of the Zoeppritz equations.* J. Appl. Geophys., **147**, 28-41, doi:10.1016/j.jappgeo.2017.10.002.

Avseth P. and Mukerji T.; 2002: *Seismic lithofacies classification from well-logs using statistical rock physics*. Petrophys., **43**, 70-81.

Avseth P., Flesche H. and Van Wijngaarden A.J.; 2003: *AVO classification of lithology and pore fluids constrained by rock physics depth trends*. The Leading Edge, **22**, 1004-1011.

Avseth P., Mukerji T. and Mavko G.; 2005: *Quantitative seismic interpretation: Applying rock physics tools to reduce interpretation risk*. Cambridge Univ. Press, Cambridge, NY, USA, 359 pp.

Bachrach R., Beller M., Liu C.C., Perdomo J., Shelander D., Dutta N. and Benabentos M.; 2004: *Combining rock physics analysis, full waveform prestack inversion and high-resolution seismic interpretation to map lithology units in deep water: a gulf of Mexico case study*. The Leading Edge, **23**, 378-383.

Bortfeld R.; 1961: *Approximations to the reflection and transmission coefficients of plane longitudinal and transverse waves*. Geophys. Prospect., **9**, 485-502, doi:10.1111/j.1365-2478.1961.tb01670.x.

Bosch M., Mukerji T. and Gonzalez E.F.; 2010: *Seismic inversion for reservoir properties combining statistical rock physics and geostatistics: a review*. Geophys., **75**, 165-176.

Buland A. and Omre, H.; 2003: *Bayesian linearized AVO inversion*. Geophys., **68**, 185-198.

Dębski W. and Tarantola, A.; 1995; *Information on elastic parameters obtained from the amplitudes of reflected waves*. Geophysics, **60**, 1426-1436.

Del Monte A.A., Corrao A., Fervari M. and Grana D.; 2011: *Seismic characterization in the Nile Delta offshore combining rock physics templates and probabilistic classification*. In: 81th Ann. Int. Meeting Expanded Abstracts, Soc. Expl. Geophys., pp. 1774-1778, doi:10.1190/1.3627549.

De Nicolao A., Drufuca G. and Rocca F.; 1993: *Eigenvalues and eigenvectors of linearized elastic inversion*. Geophys., **58**, 670-679.

Doyen P.; 2007: *Seismic reservoir characterization: an earth modelling perspective*. Eur. Ass. Geosci. Eng. Publ., The Netherlands, 255 pp.

Fatti J.L., Vail P.J., Smith G.C., Strauss P.J. and Levitt P.R.; 1994: *Detection of gas in sandstone reservoirs using AVO analysis: a 3-D seismic case history using the Geostack technique*. Geophys., **59**, 1362-1376.

Gidlow P.M., Smith G.C. and Vail P.J.; 1992: *Hydrocarbon detection using fluid factor traces: a case history.* In: Expanded Abstracts, Joint SEG/EAEG Summer Research Workshop, How useful is Amplitude-Versus-Offset (AVO) Analysis?, Big Sky, MT, U.S.A., pp. 78-89.

Goodway B.; 2001: *AVO and Lamé constants for rock parameterization and fluid detection*. CSEG Recorder, **26**, 39-60.

Goodway W., Chen T. and Downton J.; 1997: *Improved AVO fluid detection and lithology discrimination using Lamé petrophysical parameters: "Lambda-Rho," "Mu-Rho," and "Lambda/Mu fluid stack," from P and S inversions*. CSEG Recorder, **22**, 3-5.

Grana D. and Della Rossa E.; 2010: *Probabilistic petrophysical-properties estimation integrating statistical rock physics with seismic inversion.* Geophys., **75**, O21-O37.

Gray D.; 2002: *Elastic inversion for Lamé parameters*. In: Expanded Abstracts 72th Annu. Int. Meeting, Soc. Expl. Geophys., pp. 213-216.

Gray D., Goodway B. and Chen T.; 1999: *Bridging the gap: Using AVO to detect changes in fundamental elastic constants*. In: Expanded Abstracts 69th Ann. Int. Meeting, Soc. Expl. Geophys., pp. 852-855.

Lang X. and Grana D.; 2017: *Bayesian petrophysics inversion of seismic data based on linearized seismic and rock physics modeling*. In: Expanded Abstracts 87th Ann. Int. Meeting, Soc. Expl. Geophys., pp. 3087-3091.

Mazzotti A.; 1990: *Prestack amplitude analysis methodology and application to seismic bright spots in the Po Valley, Italy*. Geophys., **55**, 157-166.

Mazzotti A. and Zamboni E.; 2003: *Petrophysical inversion of AVA data*. Geophys. Prospect., **51**, 517-530.

Menke W.; 2012: *Geophysical data analysis: discrete inverse theory, Vol. 45, 3rd ed.* MATLAB edition, Academic press, Cambridge, MA, USA, 330 pp.

Mukerji T., Jørstad A., Avseth P., Mavko G. and Granli J.R.; 2001: *Mapping lithofacies and pore-fluid probabilities in a North Sea reservoir: seismic inversions and statistical rock physics*. Geophys., **66**, 988-1001.

Ostrander W.; 1984: *Plane-wave reflection coefficients for gas sands at non-normal angles of incidence*. Geophys., **49**, 1637-1648.

Richards P.G. and Frasier C.W.; 1976: *Scattering of elastic waves from depth-dependent inhomogeneities*. Geophys., **41**, 441-458.

Riedel M. and Theilen F.; 2001: *AVO investigations of shallow marine sediments*. Geophys. Prospect., **49**, 198-212.

Rutherford S.R. and Williams R.H.; 1989: *Amplitude-versus-offset variations in gas sands*. Geophys., **54**, 680-688.

Sammut C. and Webb G.I.; 2011: *Encyclopedia of machine learning*. Springer Publ. Co. Inc., New York, NY, USA, 1058 pp.

Shuey R.T.; 1985; *A simplification of the Zoeppritz equations.* Geophys., **50**, 609-614.

Stolt R.H. and Weglein A.B.; 1985: *Migration and inversion of seismic data*. Geophys., **50**, 2458-2472.

Thomas M., Ball V., Blangy J.P. and Tenorio L.; 2016: *Rock-physics relationships between inverted elastic reflectivities*. The Leading Edge, **35**, 438-444.

Verm R.W. and Hilterman F.J.; 1994: *Lithologic color-coded sections by AVO crossplots*. In: Expanded Abstracts 64th Annu. Int. Meeting, Soc. Expl. Geophys., pp. 1092-1095.

Zoeppritz K.; 1919: *On the reflection and propagation of seismic waves at discontinuities*. In: Goettinger Nachrichten (ed), Erdbebenwellen VII B, pp. 66-84.

Corresponding author: Mattia Aleardi
University of Pisa, Earth Sciences Department
Via Santa Maria 53, 56126 Pisa, Italy
Phone: +39 050 2215722; e-mail: mattia.aleardi@unipi.it